

Inversion asymmetry effects in modulation-doped $\text{Cd}_{1-x}\text{Mn}_x\text{Te}$ quantum wells

C. Rice, D. Wolverson,^{*} A. Moskalenko, and S. J. Bending
Department of Physics, University of Bath, Bath BA2 7AY, United Kingdom

G. Karczewski and T. Wojtowicz
Institute of Physics, Polish Academy of Sciences, Warsaw, Poland
 (Received 13 December 2012; published 25 March 2013)

We report a striking in-plane anisotropy of the spin-flip Raman signals observed for dilute magnetic $\text{Cd}_{1-x}\text{Mn}_x\text{Te}$ quantum wells containing a two-dimensional electron gas. The effect depends upon electron concentration, which can be varied within a single sample via secondary above-barrier illumination. The experimental results are described in a simple, single-electron picture by a model of the conduction band Hamiltonian that includes contributions from Dresselhaus, Rashba, and Zeeman terms.

DOI: [10.1103/PhysRevB.87.121304](https://doi.org/10.1103/PhysRevB.87.121304)

PACS number(s): 73.61.Ga, 73.63.Hs, 75.50.Pp, 78.30.-j

The momentum-dependent spin splittings of conduction band states arising from the action of the spin-orbit (SO) field in the absence of inversion symmetry have recently attracted a great deal of attention, especially for zinc-blende III-V semiconductor quantum wells (QWs).¹⁻⁹ However, although analogous effects are expected in zinc-blende II-VI semiconductors, they have been less well studied and fundamental parameters (for example, Dresselhaus and Rashba coefficients) have not been determined experimentally for many II-VI materials, including QWs based on CdTe, despite their relevance to spintronic devices based on high-mobility CdTe structures.¹⁰

Furthermore, dilute magnetic semiconductors (DMSs) based on CdTe and other II-VI compounds containing manganese exhibit very large conduction band spin splittings in an external magnetic field, giving a very high degree of spin polarization of the conduction band carriers.^{11,12} The interplay between inversion asymmetry effects and II-VI DMS behavior has only been studied recently theoretically¹³ and there is very little experimental information about this;¹⁴ it is often assumed that the DMS effects will mask all SO perturbations.

Here, a study of the spin-flip Raman scattering (SFRS) spectra of two-dimensional electron gases (2DEGs) within $\text{Cd}_{1-x}\text{Mn}_x\text{Te}$ QWs shows that there is a significant in-plane anisotropy of the conduction band spin splitting which arises from the combination of SO and Zeeman terms in the conduction band Hamiltonian and, therefore, the SO terms are certainly not always negligible. We describe the dependence of this anisotropy on the Fermi wave vector of the 2DEG via a simple model and indicate directions for future work.

The four QW structures were grown by molecular beam epitaxy on GaAs[001] substrates. The barriers consist of $\text{Cd}_{1-y}\text{Mg}_y\text{Te}$, $y \sim 20\%$, and each sample contains a single $\text{Cd}_{1-x}\text{Mn}_x\text{Te}$ QW of width 80, 300, 200, and 300 Å (samples 1-4, respectively). The corresponding Mn^{2+} concentrations x were 6.8%, 0.25%, and 0.79% for both samples 3 and 4, estimated by fitting the magnetic field dependence of the electron SFRS signals with a Brillouin function.¹⁵ Sample 1 is nominally undoped; samples 2-4 were modulation doped with an iodine layer located ~ 200 Å from the QW. Magneto-transport measurements showed the carrier concentrations of samples 2-4 to be of the order 10^{11} cm^{-2} , which gives a Fermi wave vector $k_F \sim 10^6 \text{ cm}^{-1}$.

Magneto-optical experiments were carried out with the sample immersed in superfluid liquid helium ($T \sim 1.5 \text{ K}$). A split coil superconducting magnet provided a magnetic field B of up to 6 T in the plane of the QW, and perpendicular to the light collection direction z . Excitation was provided by a tunable Ti-sapphire laser with a small, but nonzero, angle of incidence to the sample normal θ . This results in a finite in-plane momentum transfer to the 2DEG, $q = (2\pi/\lambda) \sin \theta$, which was of the order $q \sim 5 \times 10^4 \text{ cm}^{-1}$. The scattered light was analyzed, in crossed linear polarization $[z(\sigma\pi)\bar{z}]$, with a triple grating spectrometer with cooled CCD detection. The sample could be rotated by an angle ϕ (defined as zero for B along the in-plane direction $x = [100]$) about the normal to the QW plane. Importantly, q and B remain orthogonal independent of the angle ϕ .

Figure 1 shows SFRS spectra for samples 1 and 2 in an external magnetic field, taken at orientations of $\phi = \pi/4$ (B along $[110]$) and $\phi = 3\pi/4$ (B along $[1\bar{1}0]$). In Figs. 1(a) and 1(b), sample 1 (undoped) shows one SFRS signal, isotropic with respect to rotation by ϕ , which corresponds to the conduction band electron spin-flip energy. Figures 1(c) and 1(d) show the corresponding spectra for sample 2, which are typical of what is found for a 2DEG concentration of $\sim 3 \times 10^{11} \text{ cm}^{-2}$. Here, both collective spin-flip wave (SFW) and single-particle excitation (SPE) signals are seen, the details of which are discussed elsewhere.^{11,12,16} Figures 1(c) and 1(d) illustrate the significant anisotropy of these signals as the sample is rotated by angle ϕ .

We first rule out any effects due to an angle-dependent optical absorption, which could result in the electron and Mn^{2+} systems reaching different equilibrium temperatures T for excitation polarized along $[110]$ and $[1\bar{1}0]$ owing to different rates of optical heating. To test this, we attempted to fit the magnetic field evolution of the SFW peak position for sample 2 in both orientations A ($\phi = \pi/4$) and B ($\phi = 3\pi/4$) by varying only T . To save space we do not show the separate fits but, in Fig. 2(a), we show the difference between them (solid line, taking $T_{[110]} = 1.9 \text{ K}$ and $T_{[1\bar{1}0]} = 2.5 \text{ K}$), along with the difference between our experimental data for the same two orientations (open circles). At high fields, the interpretation based on temperature alone would predict that the anisotropy vanishes. On the contrary, we observe a finite anisotropy that persists up to our maximum field (6 T) and tends to a constant

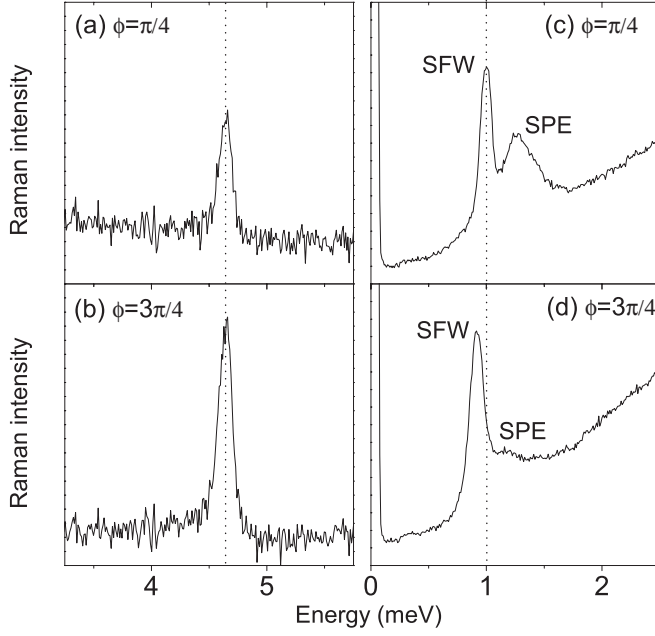


FIG. 1. Typical spin-flip Raman spectra for $\text{Cd}_{1-x}\text{Mn}_x\text{Te}$ QWs at (a), (c) $\phi = \pi/4$ and at (b), (d) $\phi = 3\pi/4$ for (a), (b) sample 1, with no 2DEG ($B = 3$ T), and (c), (d) sample 2, with a significant 2DEG concentration ($B = 5$ T). SPE: Single-particle excitation; SFW: spin-flip wave.

value (dotted line) for $B > 4$ T. We discuss the dashed line in Fig. 2(a) and the inset in Fig. 2(b) later.

Figure 2(b) shows the peak position of the SFW signal as a function of field for sample 2 in both orientations, with solid lines showing the fits from which the Mn^{2+} concentrations above were estimated; these fits indicated only a very small change in temperature but each required an additional displacement in energy arising from the anisotropic spin splitting that is of interest here.

A simple model was proposed in Ref. 14 and is extended here. The spin-dependent SO term in the conduction band Hamiltonian depends on k^3 as follows:^{7,17}

$$\mathcal{H} = \beta[\sigma_x k_x (k_y^2 - k_z^2) + \sigma_y k_y (k_z^2 - k_x^2) + \sigma_z k_z (k_x^2 - k_y^2)]. \quad (1)$$

The $\sigma_{x\dots z}$ are the 2×2 Pauli spin matrices. For a QW structure with growth axis along z , it is usual to replace k_z and k_z^2 by their expectation values $\langle k_z \rangle = 0$ and $\langle k_z^2 \rangle = \kappa^2 \neq 0$,^{3,17} respectively. Equation (1) then gives

$$\mathcal{H}_{\text{BIA}} = \beta\kappa^2(\sigma_y k_y - \sigma_x k_x) + \beta k_x k_y (\sigma_x k_y - \sigma_y k_x). \quad (2)$$

The Dresselhaus¹⁸ or bulk inversion asymmetry (BIA) Hamiltonian \mathcal{H}_{BIA} is dependent on the band-structure parameter β and on the QW width L , since $\kappa \sim \pi/L$ (discussed in detail in Refs. 19 and 20). Frequently, one can include only the first term of Eq. (2), which is linear in k , but here, the presence of the 2DEG leads to values of $k_x, k_y \sim k_F$ that can be comparable to κ and so the second term of \mathcal{H}_{BIA} should be retained.

Another symmetry-reducing effect is the built-in electric field arising from the asymmetric modulation doping of our QWs.^{7,21–23} This Rashba,²⁴ or structural inversion asymmetry

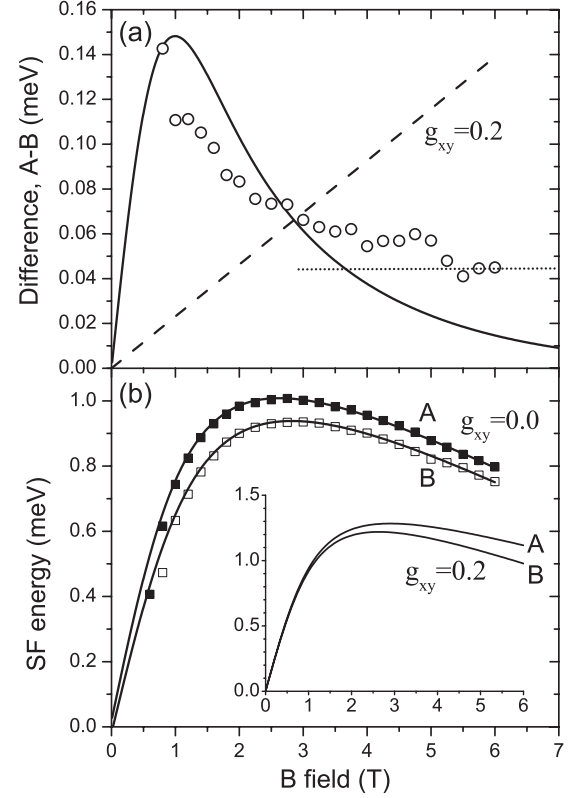


FIG. 2. (a) Predicted difference (solid line) between the peak positions of the SFW signals for sample 2 in orientations A ($\phi = \pi/4$) and B ($\phi = 3\pi/4$) assuming only a change in temperature; experimental data: open circles. Dashed line: Predicted difference with an anisotropic g factor only. (b) Peak positions of the SFW signals for orientations A (solid squares) and B (open squares), with fits (solid lines) including a vertical shift and no temperature change. Inset: Predicted peak positions of the SFW signals in the two orientations on the basis of an anisotropic g factor only.

(SIA) term, has the following Hamiltonian:

$$\mathcal{H}_{\text{SIA}} = \alpha(\sigma_x k_y - \sigma_y k_x), \quad (3)$$

where α is the Rashba splitting parameter, which is dependent on the QW band structure and on the magnitude of the electric field (for recent discussions, see Refs. 7 and 25). Next, we include the Zeeman term for an in-plane magnetic field,

$$\mathcal{H}_Z = (g^* \mu_B / 2)(\sigma_x B_x + \sigma_y B_y), \quad (4)$$

where g^* is the B - and T -dependent effective gyromagnetic ratio that is the sum of the isotropic band-structure CdTe g factor of $g_{xx} = g_{yy} = -1.67$,²⁶ and its enhancement due to the s - d exchange interaction between band electrons and Mn^{2+} ions in the DMS; μ_B is the Bohr magneton. Finally, an in-plane anisotropy of the band-structure g factor ($g_{xy} = g_{yx} \neq 0$) can arise from the combined action of the potential gradient across the QW and the in-plane magnetic field,^{27–29} and this term will be linear in B :

$$\mathcal{H}_{xy} = (g_{xy} \mu_B / 2)(\sigma_x B_y + \sigma_y B_x). \quad (5)$$

To solve the total Hamiltonian, $\mathcal{H}_T = \mathcal{H}_{\text{BIA}} + \mathcal{H}_{\text{SIA}} + \mathcal{H}_Z + \mathcal{H}_{xy}$, we use the fact that the in-plane momentum

transfer is small compared to the Fermi wave vector, $q \ll k_F$, and therefore the initial and final states in the SFRS process have momenta that remain close in magnitude to k_F . Although a wide range of carrier states near the Fermi energy can participate in the scattering process, we simplify the problem by noting that their mean orientation is parallel to q . Therefore, the in-plane momentum can be approximated by $(k_x, k_y) \simeq k_F(\cos \phi, \sin \phi)$, and the magnetic field is written as $(B_x, B_y) = B_0(-\sin \phi, \cos \phi)$. In the absence of the external magnetic field, the problem is analytically soluble.^{30,31} Here, however, the Zeeman term \mathcal{H}_Z of our DMS QWs dominates (except at very low fields) and a full analytic solution is too large to reproduce here. For an illustrative result which will help interpret the data, we expand the eigenvalues E_{\pm} of \mathcal{H}_T (taking $g_{xy} = 0$ for now) and obtain Eq. (6), valid only in the high-field limit:

$$E_{\pm} = \pm \{g\mu_B B/2 + \beta(2\kappa^2 k_F - k_f^3) \cos \phi \sin \phi - \alpha k_F\}. \quad (6)$$

To justify taking this limit, we note that a typical magnitude at $B = 4$ T of the isotropic band-structure Zeeman splitting is $g_{xx}\mu_B B \sim 0.4$ meV, the DMS s - d exchange splitting ranges from 1 to 4 meV (depending on x), and all other terms are expected to be of order 0.3 meV or less. However, we simulate our data without this approximation, by finding the eigenvalues of \mathcal{H}_T numerically, including also a finite contribution from \mathcal{H}_{xy} . There are only a few discussions of the combination of an in-plane magnetic field with SO effects and these mostly present numerical solutions with parameters relevant to III-V QWs.^{32–34}

We now look for evidence that the twofold rotational symmetry of the SFW shift ($E_+ - E_-$) depends on k_F , as predicted by both the full numerical solution and the model of Eq. (6). We consider only the SFW signal [see Fig. 1(b)], whose behavior is more nearly single-electron-like.^{11,16,35} To test the attribution of the observed SFW anisotropy to BIA and SIA effects, we modified the carrier concentration using above-barrier (532 nm) excitation.³⁶ Fitting the photoluminescence (PL) line shape gave an estimate of the QW carrier concentration, and therefore also of the Fermi energy and wave vector.³⁷ For this sample, above-barrier excitation reduces the electron concentration in the QW.

In Fig. 3 we show the anisotropy of the SFW signal, recorded at 4 T, for three different above-barrier illumination powers (increasing by a factor of ~ 3) and with constant low power resonant excitation; we show data for samples 2 and 3 (sample 4 displays a similar anisotropy). Two effects are observed as the above-barrier illumination power is increased; first, there is a decrease in amplitude of the anisotropy, and second, there is a move of the mean SFRS shift of the SFW signal to higher energy. We emphasize that any heating effects, which would increase with increasing illumination power, would *decrease* the dominant DMS Zeeman term in the SFRS shift, opposite to what is seen in Fig. 3.

Each data set of Fig. 3 was simulated with the values of k_F derived from the PL line shapes used as input; the results contain an isotropic part plus a term in $\sin \phi \cos \phi$, as implied by the form of Eq. (6). For example, for the innermost curve of Fig. 3(b), $k_F = 1.4 \times 10^6$ cm⁻¹ (0.014 Å⁻¹). From the

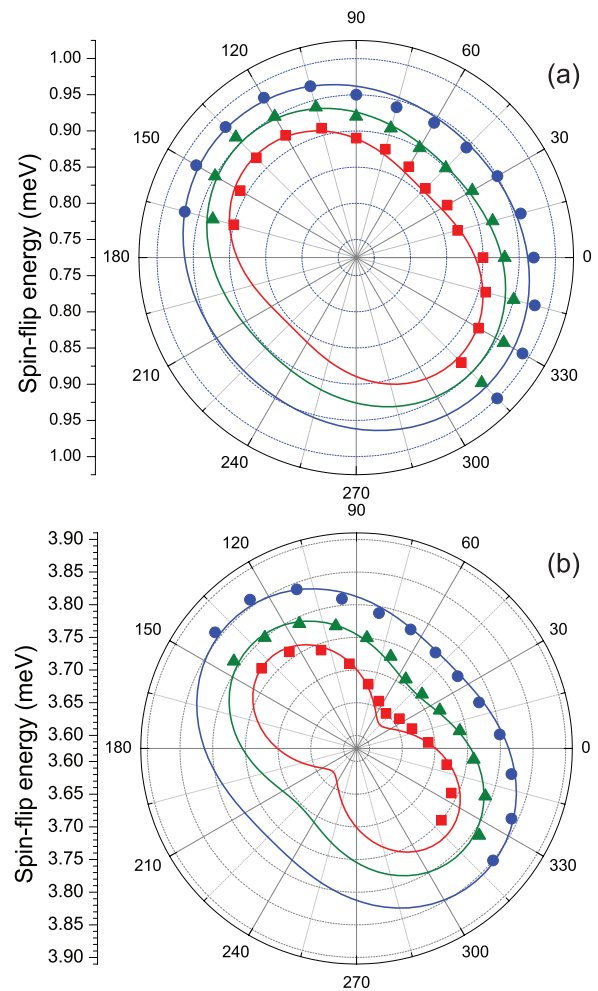


FIG. 3. (Color online) Dependence on angle of the SFW peak position at $B = 4$ T for (a) sample 2 and (b) sample 3 with resonant excitation of the QW and additional above-barrier illumination (whose power increases in the sequence red squares, green triangles, blue circles). Solid lines are simulations of the data. The vertical (radial) scale excludes the origin to give an expanded view of the region of interest.

solution for the single-particle QW electron wave function, we find $\kappa^2 = 1.6 \times 10^{-4}$ Å⁻², consistent with the estimate $\kappa \sim \pi/L$. Our simulations lead to an estimate of 45 ± 5 eV Å³ for the coefficient of the Dresselhaus (BIA) term β , for CdTe, using the same value to fit data from both samples. This is in agreement with a value of $\vec{k} \cdot \vec{p}$ perturbation theory of 43.88 eV Å³ in Ref. 7. However, our estimate does not agree well with more recent *ab initio* predictions³⁸ or estimates following Ref. 39 (8.5 and 11.7 eV Å³, respectively). Recently, it has been shown that many-body collective effects can significantly enhance SO fields in non-DMS III-V QWs,⁴⁰ in that case by about a factor of five, which would explain the present discrepancy; this question needs to be addressed also in II-VI DMS QWs.

As Fig. 3 suggests, the above-barrier beam reduces the 2DEG concentration and therefore also reduces k_F . The variation of the SFW signal with k_F was therefore measured at fixed angle and field while varying the above-barrier beam power incident on the sample ($B = 4$ T and $\phi = \pi/4, \pi/2$,

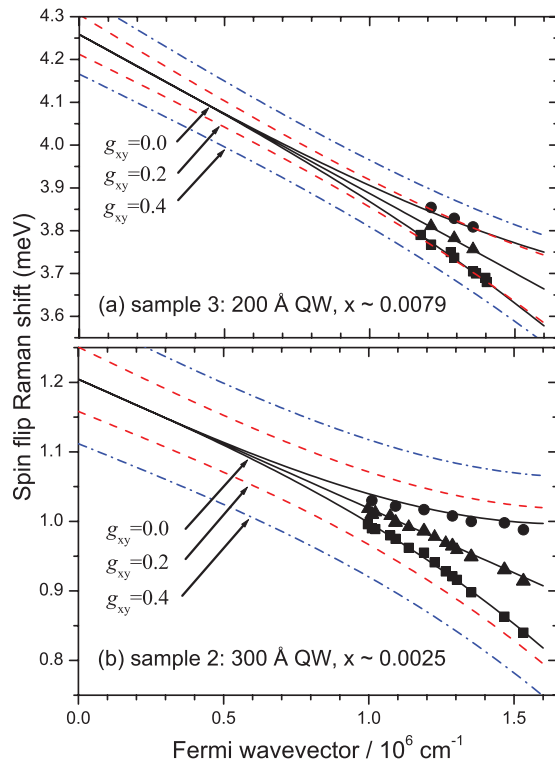


FIG. 4. (Color online) Variation of the SFW peak position with Fermi wave vector k_F for (a) sample 3 and (b) sample 2 at fixed orientation (squares: $\phi = \pi/4$; triangles: $\phi = \pi/2$; circles: $\phi = 3\pi/4$) and $B = 4$ T. The solid, dashed, and dashed-dotted lines show simulations for g_{xy} increasing from zero.

and $3\pi/4$). The results for samples 2 and 3 are shown in Fig. 4, together with numerical simulations. The size of the SIA term α was obtained from the gradient for $\phi = \pi/2$

where, as Eq. (6) shows, the anisotropic part of the splitting is zero. The SIA term can in principle be calculated following Ref. 5 given a self-consistent solution for the electric field across the QW, but here we take it as a free parameter and obtain values of 18 and 37 ± 2 meV Å for samples 2 and 3, respectively, larger than typical results on nonmagnetic QWs (e.g., 6.9 meV Å in a GaAs-based QW⁴), due to the anisotropic modulation doping. In the future, it would be interesting to test the present model by the use of symmetrical modulation doping to reduce this term. The BIA term is revealed by the nonlinear dependence of the splitting on k_F for $\phi = \pi/4, 3\pi/4$ (using again $\beta \sim 45 \pm 5$ eV Å³; the smaller value of Ref. 38 does not give a strong enough curvature). Finally, we show simulations for a range of values of g_{xy} ; any value $g_{xy} \leq 0.2$ would be consistent with the k_F -dependent data for sample 3 and $g_{xy} \leq 0.1$ for sample 2. On varying the magnetic field, there is no indication of a nonzero g_{xy} ; the inset in Fig. 2(b) shows the expected magnetic field dependence of the SFW peak positions for $\phi = \pi/4, 3\pi/4$ taking $g_{xy} = 0.2$; the dashed line in Fig. 2(a) shows that the difference between these would grow linearly with field, contrary to what we observe.

In summary, we observe a significant in-plane anisotropy of the conduction band spin splitting in $\text{Cd}_{1-x}\text{Mn}_x\text{Te}$ QW samples containing 2DEGs. The magnitude of the anisotropy is found to be field independent for large fields and varies with the 2DEG concentration. The data are described by a model involving both Rashba and Dresselhaus terms in combination with a large Zeeman splitting and so the influence of spin-orbit fields is shown not to be negligible even in DMS QWs.

We acknowledge the support of the Leverhulme Trust (Grant No. F/00 351/W). We thank Paweł Pfeffer for helpful comments on this work. Research in Poland was partially supported by the National Science Centre (Poland) under Grant No. DEC-2012/06/A/ST3/00247.

*d.wolverson@bath.ac.uk

¹B. Das, S. Datta, and R. Reifenberger, *Phys. Rev. B* **41**, 8278 (1990).

²B. Jusserand, D. Richards, H. Peric, and B. Etienne, *Phys. Rev. Lett.* **69**, 848 (1992).

³D. Richards, B. Jusserand, H. Peric, and B. Etienne, *Phys. Rev. B* **47**, 16028 (1993).

⁴B. Jusserand, D. Richards, G. Allan, C. Priester, and B. Etienne, *Phys. Rev. B* **51**, 4707 (1995).

⁵P. Pfeffer, *Phys. Rev. B* **59**, 15902 (1999).

⁶P. Pfeffer and W. Zawadzki, *Phys. Rev. B* **59**, R5312 (1999).

⁷R. Winkler, *Spin-Orbit Coupling Effects in Two-Dimensional Electron and Hole Systems* (Springer, Berlin, 2003).

⁸W. Zawadzki and P. Pfeffer, *Semicond. Sci. Technol.* **19**, R1 (2004).

⁹X. Cartoixà, L.-W. Wang, D. Z.-Y. Ting, and Y.-C. Chang, *Phys. Rev. B* **73**, 205341 (2006).

¹⁰C. Betthausen, T. Dollinger, H. Saarikoski, V. Kolkovsky, G. Karczewski, T. Wojtowicz, K. Richter, and D. Weiss, *Science* **337**, 324 (2012).

¹¹B. Jusserand, F. Perez, D. R. Richards, G. Karczewski, T. Wojtowicz, C. Testelin, D. Wolverson, and J. J. Davies, *Phys. Rev. Lett.* **91**, 086802 (2003).

¹²F. Perez, C. Aku-leh, D. Richards, B. Jusserand, L. C. Smith, D. Wolverson, and G. Karczewski, *Phys. Rev. Lett.* **99**, 026403 (2007).

¹³T. Tsuchiya, *J. Phys. Soc. Jpn.* **81**, 094706 (2012).

¹⁴C. Rice, D. Wolverson, A. Moskalenko, S. J. Bending, G. Karczewski, and T. Wojtowicz, *Phys. Status Solidi C* **9**, 1783 (2012).

¹⁵J. A. Gaj, R. Planel, and G. Fishman, *Solid State Commun.* **29**, 435 (1979).

¹⁶F. Perez, J. Cibert, M. Vladimirova, and D. Scalbert, *Phys. Rev. B* **83**, 075311 (2011).

¹⁷E. L. Ivchenko, *Optical Spectroscopy of Semiconductor Nanostructures* (Alpha Science, Harrow, 2005).

¹⁸P. D. Dresselhaus, C. M. A. Papavassiliou, R. G. Wheeler, and R. N. Sacks, *Phys. Rev. Lett.* **68**, 106 (1992).

¹⁹P. Pfeffer and W. Zawadzki, *Phys. Rev. B* **74**, 233303 (2006).

²⁰M. P. Walser, U. Siegenthaler, V. Lechner, D. Schuh, S. D. Ganichev, W. Wegscheider, and G. Salis, *Phys. Rev. B* **86**, 195309 (2012).

²¹P. S. Eldridge, W. J. H. Leyland, P. G. Lagoudakis, O. Z. Karimov, M. Henini, D. Taylor, R. T. Phillips, and R. T. Harley, *Phys. Rev. B* **77**, 125344 (2008).

- ²²P. S. Eldridge, W. J. H. Leyland, P. G. Lagoudakis, R. T. Harley, R. T. Phillips, R. Winkler, M. Henini, and D. Taylor, *Phys. Rev. B* **82**, 045317 (2010).
- ²³P. S. Eldridge, J. Hübner, S. Oertel, R. T. Harley, M. Henini, and M. Oestreich, *Phys. Rev. B* **83**, 041301 (2011).
- ²⁴Y. A. Bychkov and E. I. Rashba, *J. Phys. C* **17**, 6039 (1984).
- ²⁵U. Ekenberg and D. M. Gvozdić, *Phys. Rev. B* **78**, 205317 (2008).
- ²⁶S. Tsoi, I. Miotkowski, S. Rodriguez, A. K. Ramdas, H. Alawadhi, and T. M. Pekarek, *Phys. Rev. B* **69**, 035209 (2004).
- ²⁷V. K. Kalevich and V. L. Korenev, *JETP Lett.* **57**, 571 (1993).
- ²⁸Y. A. Nefyodov, A. V. Shchepetilnikov, I. V. Kukushkin, W. Dietsche, and S. Schmult, *Phys. Rev. B* **84**, 233302 (2011).
- ²⁹D. J. English, J. Hübner, P. S. Eldridge, D. Taylor, M. Henini, R. T. Harley, and M. Oestreich, *Phys. Rev. B* **87**, 075304 (2013).
- ³⁰E. A. de Andrada e Silva, *Phys. Rev. B* **46**, 1921 (1992).
- ³¹R. Winkler, *Phys. Rev. B* **69**, 045317 (2004).
- ³²M. Valín-Rodríguez and R. G. Nazmitdinov, *Phys. Rev. B* **73**, 235306 (2006).
- ³³E. P. Nakhmedov and O. Alekperov, *Eur. Phys. J. B* **85**, 298 (2012).
- ³⁴C. Micu and E. Papp, *Superlattices Microstruct.* **51**, 651 (2012).
- ³⁵P. M. Shmakov, A. P. Dmitriev, and V. Y. Kachorovskii, *Phys. Rev. B* **83**, 233204 (2011).
- ³⁶A. V. Koudinov, Y. G. Kusrayev, D. Wolverson, L. C. Smith, J. J. Davies, G. Karczewski, and T. Wojtowicz, *Phys. Rev. B* **79**, 241310 (2009).
- ³⁷C. Aku-Leh, F. Perez, B. Jusserand, D. Richards, W. Pacuski, P. Kossacki, M. Menant, and G. Karczewski, *Phys. Rev. B* **76**, 155416 (2007).
- ³⁸A. N. Chantis, M. van Schilfgaarde, and T. Kotani, *Phys. Rev. Lett.* **96**, 086405 (2006).
- ³⁹M. Cardona, N. E. Christensen, and G. Fasol, *Phys. Rev. B* **38**, 1806 (1988).
- ⁴⁰F. Baboux, F. Perez, C. A. Ullrich, I. D'Amico, J. Gómez, and M. Bernard, *Phys. Rev. Lett.* **109**, 166401 (2012).